Volume 16
Number 19
21 May 2025
Pages 8139–8596

Chemical Science

rsc.li/chemical-science

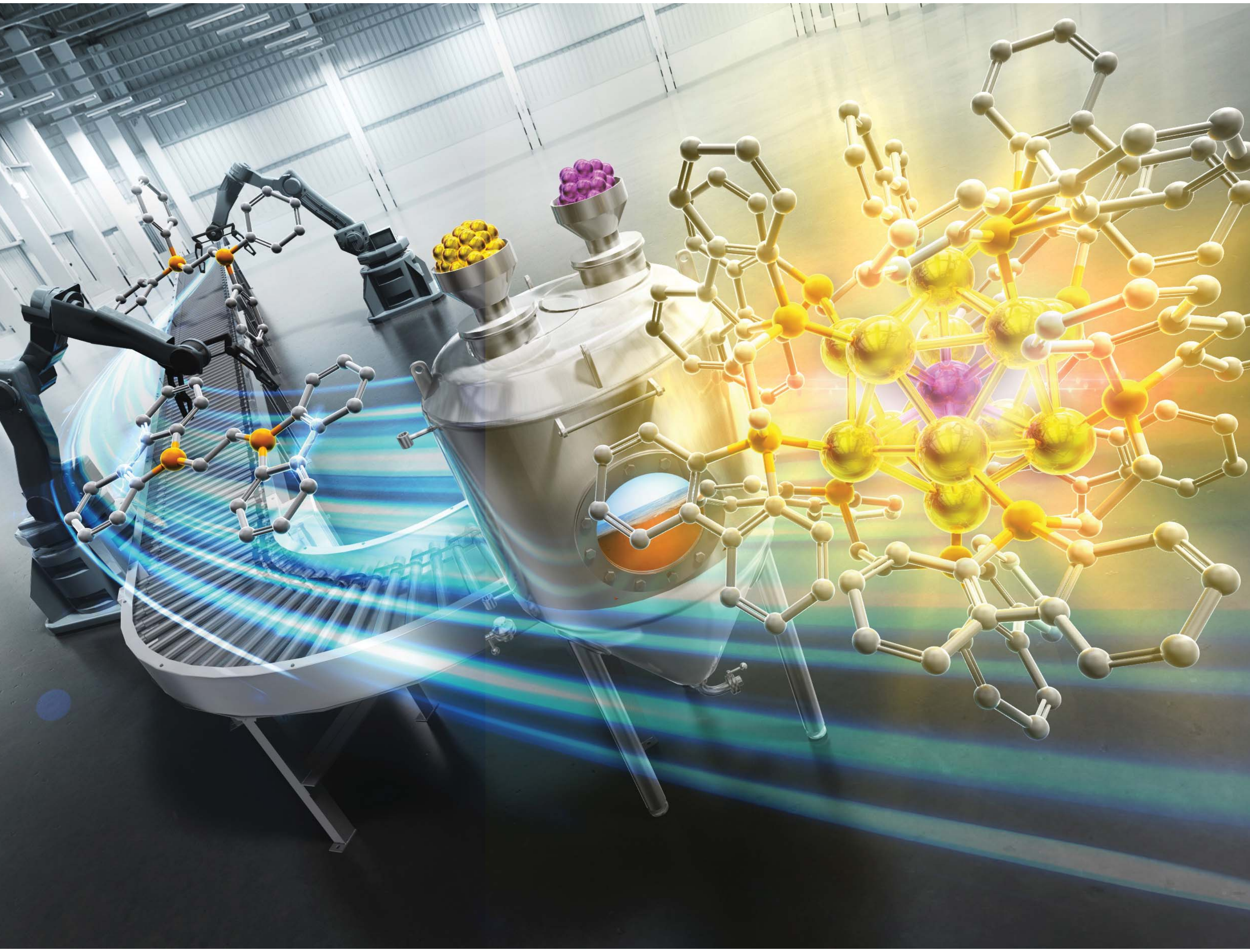

ISSN 2041-6539

ROYAL SOCIETY
OF **CHEMISTRY**

EDGE ARTICLE
Katsuya Mutoh, Tatsuya Tsukuda, Takuya Nakashima *et al.*
A nearly perfect icosahedral Ir@Au$_{12}$ superatom with superior photoluminescence obtained by ligand engineering

15 YEARS ANNIVERSARY

Chemical
Science

ROYAL SOCIETY
OF CHEMISTRY

EDGE ARTICLE

View Article Online
View Journal | View Issue

Check for updates

Cite this: *Chem. Sci.*, 2025, **16**, 8240

All publication charges for this article have been paid for by the Royal Society of Chemistry

Received 22nd January 2025
Accepted 28th March 2025

DOI: 10.1039/d5sc00561b

rsc.li/chemical-science

A nearly perfect icosahedral Ir@Au_{12} superatom with superior photoluminescence obtained by ligand engineering†

Katsuya Mutoh, *[a] Teppei Yahagi,[a] Shinjiro Takano, [b] Sonomi Kawakita,[a] Takeshi Iwasa, [cd] Tetsuya Taketsugu, [cd] Tatsuya Tsukuda *[b] and Takuya Nakashima *[a]

Heterometal doping and the introduction of surface ligands drastically alter the optical and photophysical properties of gold-based superatoms by modulating their electronic structures and the excited state dynamics. In this study, we investigate how the structures and the optical properties of an Ir@Au_{12} superatom capped by a diphosphine ligand, bis[benzo[*b*]phosphindole]ethane (bbpe), in which the rotation of the phenyl groups is prohibited, differ from those capped by the conventional diphosphine ligands, such as 1,2-bis(diphenylphosphino)ethane (dppe) and bis(diphenylphosphino)methane (dppm). The co-reduction of Ir(III)- and Au(I)-precursors under mild reaction conditions yielded homoleptically capped $[IrAu_{12}(bbpe)_6]^{3+}$ clusters (**$IrAu_{12}$-b**) as the primary product. Single crystal X-ray diffraction analysis of **$IrAu_{12}$-b** revealed the formation of a nearly perfect icosahedral Ir@Au_{12} superatomic core, in which the central Ir atom is equidistant from each vertex Au atom. The energy gap between occupied 1P and unoccupied 1D superatomic orbitals of **$IrAu_{12}$-b** was larger than that of its dppm-capped counterpart, $[IrAu_{12}(dppm)_6]^{3+}$ as evidenced by a blue shift (140 nm) of the photoluminescence (PL) wavelength and DFT calculations. **$IrAu_{12}$-b** exhibited PL at 596 nm with a high quantum yield of 87% in deaerated CH_2Cl_2 due to the expanded 1P–1D energy gap and the restricted molecular motions of the bbpe ligands.

Introduction

Atomically precise metal clusters possess size-specific electronic structures characterized by discrete energy levels, just like atoms and molecules. As a result, they exhibit novel physicochemical properties that differ from their bulk and nanoparticle counterparts and have attracted attention not only for fundamental research but also for various applications.[1–12] For example, gold clusters with clear energy gaps between the highest occupied molecular orbital (HOMO) and the lowest unoccupied molecular orbital (LUMO) have been demonstrated to exhibit attractive photofunctions, including photoluminescence (PL), circularly polarized luminescence (CPL), triplet sensitization, and photocatalysis.[13–20] The widely reported icosahedral Au_{13} cluster has been considered a representative superatom.[21–25] Direct stabilization of the Au_{13} superatom with phosphines and *N*-heterocyclic carbenes (NHCs), without forming Au(I)-ligand staple motifs, often leads to pronounced PL in the red to near-infrared region.[21,26–30] The heteroatom doping further perturbs the superatomic orbitals, resulting in the drastic modulation of the HOMO–LUMO energy gaps (HL gaps).[30–38] The diphosphine-protected Au_{13} clusters such as $[Au_{13}(dppm)_6]^{5+}$ (dppm: bis(diphenylphosphino)methane) and $[Au_{13}(dppe)_5Cl_2]^{3+}$ (dppe: 1,2-bis(diphenylphosphino)ethane) serve as a platform for the heteroatom doping.[33–40] The latter has been further modified by the exchange reaction of the Cl ligands with other halogens, alkynyl and subsequently isocyanide ligands.[41–43]

The ligand shell is not only involved in controlling the geometry of the superatomic cores, but also affects their electronic structures and photophysical processes.[44–47] More specifically, the interactions of the ligand with the superatomic core and the adjacent ligands are crucial for controlling the HL gap and the excited state dynamics of the cores. For example, Lu *et al.* reported a ligand-induced contraction of the Au_{13} core

---

[a] Department of Chemistry, Graduate School of Science, Osaka Metropolitan University, Sumiyoshi-ku, Osaka 558-8585, Japan. E-mail: mutoh@omu.ac.jp; takuya.nakashima@omu.ac.jp

[b] Department of Chemistry, Graduate School of Science, The University of Tokyo, Bunkyo-ku, Tokyo 113-0033, Japan. E-mail: tsukuda@chem.s.u-tokyo.ac.jp

[c] Department of Chemistry, Faculty of Science, Hokkaido University, North 10 West 5, Sapporo, Hokkaido 060-0810, Japan

[d] WPI-ICReDD, Hokkaido University, Sapporo, Hokkaido, 060-0810, Japan

† Electronic supplementary information (ESI) available: Synthesis, ^1H NMR spectrum, PLQY and lifetime measurements, DPV measurement, NBO analysis, and the other experimental and DFT calculation results. X-ray crystallographic data, CCDC 2415728. For ESI and crystallographic data in CIF or other electronic format see DOI: https://doi.org/10.1039/d5sc00561b

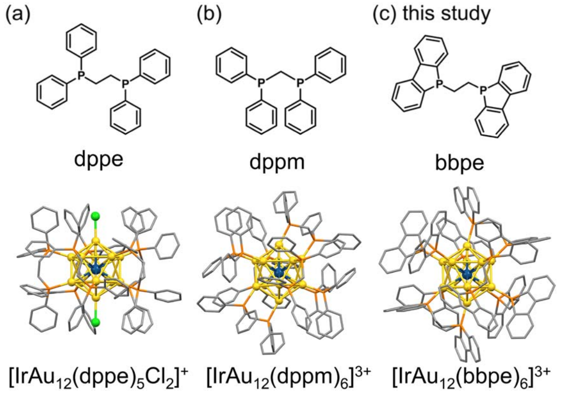

Fig. 1 The molecular structures of the diphosphine ligands and the corresponding Ir@Au$_{12}$ clusters for (a) [IrAu$_{12}$(dppe)$_5$Cl$_2$]$^+$ (**IrAu$_{12}$-e-Cl**), (b) [IrAu$_{12}$(dppm)$_6$]$^{3+}$ (**IrAu$_{12}$-m**) and (c) [IrAu$_{12}$(bbpe)$_6$]$^{3+}$ (**IrAu$_{12}$-b**).

leading to an expansion of the HL gap and a significant increase in the PL quantum yield (QY).[48] The use of *N*,*N*′-dibenzyl-substituted benzimidazolium NHC ligands rigidifies the Au$_{13}$ superatom through multiple CH–π and π–π interactions in the ligand layer, also resulting in high PLQYs.[45,49] In contrast to the recent successful applications of various NHC ligands,[50–53] less systematic studies have been conducted for the diphosphine molecules as capping ligands for the Au$_{13}$ superatoms.

Bis[benzo[*b*]phosphindole]ethane (bbpe) is a derivative of dppe in which the two phenyl rings are fused by a chemical bond (Fig. 1).[45] Since the benzo[*b*]phosphindole (bp) framework of bbpe rigidly links the phenyl rings into a planar structure, the degree of freedom of the aromatic units is significantly restricted. This simple chemical modification suppresses the vibrational and rotational modes that can have a significant impact on the relaxation process of the photo-excited state of the Au$_{13}$ superatoms. Motivated by our recent development of highly luminescent [IrAu$_{12}$(dppe)$_5$Cl$_2$]$^+$ cluster (**IrAu$_{12}$-e-Cl**),[35] in this study, we used bbpe as a ligand to stabilize Ir@Au$_{12}$ superatoms with the intention of further enhancing their PL property (Fig. 1). The cluster synthesis with bbpe unexpectedly yielded a Cl-free cluster [IrAu$_{12}$(bbpe)$_6$]$^{3+}$ (**IrAu$_{12}$-b**) as the main product. The homoleptic capping of the Ir@Au$_{12}$ core with six bbpe ligands resulted in an almost perfect icosahedral structure. Due to the expanded HL gap as well as the suppressed non-radiative relaxation pathways of the excited state, **IrAu$_{12}$-b** exhibited bright PL at 596 nm with PLQY as high as 0.87. The remarkable roles of the bbpe ligands on the PL properties of **IrAu$_{12}$-b** are discussed by comparing the geometry and optical properties of [IrAu$_{12}$(dppm)$_6$]$^{3+}$ (**IrAu$_{12}$-m**) as a reference (Fig. 1).

Results and discussion

Synthesis and structure analysis

The detailed synthetic procedure of **IrAu$_{12}$-b** is given in the ESI.† The bbpe ligand and the corresponding gold complex, Au$_2$(bbpe)Cl$_2$, were synthesized according to the literature procedure.[54] The mixture of Au$_2$(bbpe)Cl$_2$ and [Ir(COD)Cl]$_2$ (COD: 1,5-cyclooctadiene) was co-reduced in CH$_2$Cl$_2$. While a typical reduction condition using NaBH$_4$ at room temperature did not produce any luminescent species, the milder condition using borane-*tert*-butylamine complex[26,55,56] at 273 K yielded a luminescent solution. The larger agglomerates in the as-synthesized solution were removed by a reverse-phase column chromatography (Wakosil 100C18, Wako-Fuji Film) using a methanol solution containing 0.1 vol% trifluoroacetic acid (TFA) and 0.1 vol% diethylamine (DEA) as an eluent.[57] The pretreated sample was then analyzed by HPLC using a C$_{30}$ reverse-phase column (GL Sciences Inc.) as shown in Fig. S1a.† Five well-separated peaks were observed, and three fractions with retention times of 11, 25, and 29 min (peaks 1, 3, and 4 in Fig. S1a,† respectively) contained luminescent species. Electrospray ionization (ESI) mass spectrometry of the HPLC fractions (Fig. S1b†) showed that the major fraction (peak 1 in Fig. S1a†) contained the target cluster (**IrAu$_{12}$-b**) and that another minor fraction (peak 4 in Fig. S1†) was contaminated by other species such as [IrAu$_{12}$(bbpe)$_5$Cl$_2$]$^+$ (Fig. S2†). The PL maxima for peaks 1, 3, and 4 were 598, 632, and 642 nm, respectively (Fig. S1c†). It should be noted that gold clusters with visible PL could not be obtained without [Ir(COD)Cl]$_2$ in the synthesis.

Since **IrAu$_{12}$-b** showed the brightest PL among the species obtained, the main fraction (peak 1) was subjected to isolation by a preparative HPLC cycle, followed by recrystallization after treating the solution with NaPF$_6$. The geometrical structure of **IrAu$_{12}$-b** was determined by single crystal X-ray diffraction (SCXRD) analysis (Fig. 2a). The Ir@Au$_{12}$ superatomic core was protected by six bbpe ligands with a coordination pattern, similar to that of **IrAu$_{12}$-m.**[34] However, the superatomic core of **IrAu$_{12}$-b** has a higher symmetry than that of **IrAu$_{12}$-m.** A singlet peak in the ^{31}P{^{1}H} NMR spectrum of **IrAu$_{12}$-b** indicates that Ir atom is located at the center of the Ir@Au$_{12}$ core (Fig. S3†).[35] The symmetric coordination of bbpe ligands to the Ir@Au$_{12}$ core of **IrAu$_{12}$-b** was also suggested by a simple peak pattern in the ^{1}H NMR spectrum (Fig. S4†). The bond lengths in the Ir@Au$_{12}$ core were compared between **IrAu$_{12}$-b** and **IrAu$_{12}$-m** (Fig. 2b, c and Table 1). Surprisingly, all the Ir–Au distances in **IrAu$_{12}$-b** are identical (2.7397 ± 0.0003 Å), and the distribution of the Au–Au distances is remarkably narrower than that of **IrAu$_{12}$-m.** Since the average Ir–Au and Au–Au bond lengths of **IrAu$_{12}$-b** and **IrAu$_{12}$-m** are very similar (Table 1), the narrower

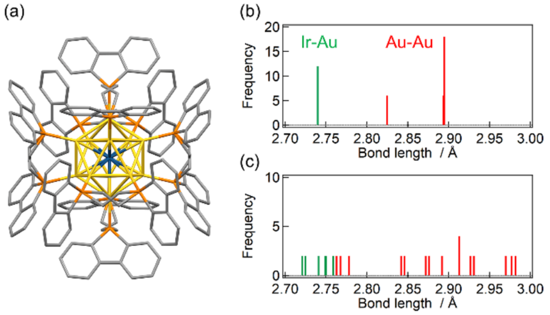

Fig. 2 (a) The structure of IrAu$_{12}$-b determined by SCXRD. (b and c) Bond length distributions in (b) IrAu$_{12}$-b and (c) IrAu$_{12}$-m. Color code: yellow, Au; dark blue, Ir; orange, P; gray, C.

Table 1 Structural Data of IrAu$_{12}$-b and IrAu$_{12}$-m Obtained by SCXRD Analysis

	Ir–Au (Å)	Au–Au (Å)	Au–P (Å)	CSM
IrAu$_{12}$-b	2.740 ± 0.000	2.881 ± 0.028	2.285 ± 0.002	0.014
IrAu$_{12}$-m (ref. 40)	2.741 ± 0.014	2.883 ± 0.072	2.301 ± 0.013	0.091

bond length distributions for **IrAu$_{12}$-b** indicate the formation of a higher symmetric icosahedron of Ir@Au$_{12}$ by the protection with bbpe. The formation of a nearly ideal icosahedral Ir@Au$_{12}$ core in **IrAu$_{12}$-b** was also confirmed by a much smaller continuous symmetry measure (CSM) value than that of **IrAu$_{12}$-m** (Table 1). To the best of our knowledge, the CSM value of 0.014 is comparable to the smallest one (0.013) for the Pd@Au$_{12}$ core of $[\mathrm{PdAu_{12}(dppe)_5(C{\equiv}CPh)_2}]^{2+}$ (**PdAu$_{12}$-e-PA**)[43] among the series of M@Au$_{12}$ superatoms reported to date (Table S1†). Nonetheless, the dopant Pd atom is not situated at the very center of icosahedron in **PdAu$_{12}$-e-PA** (Pd–Au: 2.731 ± 0.020 Å).[43] The ethylene bridge between the coordinative phosphorous atoms in bbpe may relax the structural strain observed in **IrAu$_{12}$-m** where the less flexible methylene bridge imposes constraints incompatible with the surface Au–Au bonds in the Ir@Au$_{12}$ core. In the case of bbpe, the more rigid bp unit may affect the ethylene bride conformation, which further influences the distance and orientation of phosphorous atoms on the surface of the Ir@Au$_{12}$ core. The coordination of six bbpe forms a cuboidal (hexahedral) cage surrounding the icosahedral core (Fig. 2a).

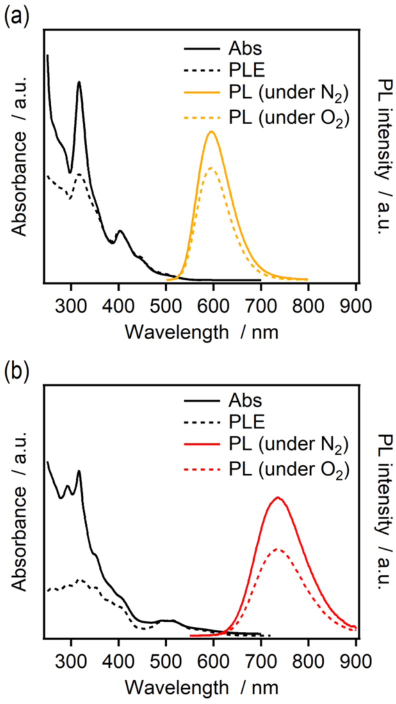

Fig. 3 UV-vis absorption, photoluminescence and excitation spectra of (a) IrAu$_{12}$-b and (b) IrAu$_{12}$-m in CH$_2$Cl$_2$.

Optical properties

The ligand effect on the electronic structure of the Ir@Au$_{12}$ core was investigated by UV-vis absorption and luminescence spectroscopy. Fig. 3 shows the absorption, PL, and excitation spectra of **IrAu$_{12}$-b** and **IrAu$_{12}$-m** in CH$_2$Cl$_2$. The absorption onset and PL peak ($\lambda_{\max}$) of **IrAu$_{12}$-b** were blue-shifted by ∼100 and ∼139 nm, respectively, from those of **IrAu$_{12}$-m.**[34] These results indicate that the HL gap of **IrAu$_{12}$-b** is larger than that of **IrAu$_{12}$-m**. The PL was assigned to the excited triplet state-based phosphorescence since the PL intensity decreases in the presence of molecular oxygen. Notably, the slight modification of the ligand structure from dppm to bbpe drastically enhanced the PL efficiency. The PLQY of **IrAu$_{12}$-b** was 0.870 in deaerated CH$_2$Cl$_2$ determined by the absolute method (JASCO, ILF-135), while that of **IrAu$_{12}$-m** was reported to be 0.14.[40] This PLQY is among the highest reported for the icosahedral M@Au$_{12}$ clusters.[30] The PLQY did not show a clear dependence on the solvent polarity (Table S2 and Fig. S5†). The PL lifetime of **IrAu$_{12}$-b** in CH$_2$Cl$_2$ was determined to be 4.18 μs (Table 2 and Fig. S6†), which is slightly longer than that of **IrAu$_{12}$-m** (3.6 μs).[40] The rate constants for the PL (k_r) and the nonradiative process (k_nr) of **IrAu$_{12}$-b** were calculated to be 2.1×10^5 and 3.1×10^4 s^{-1}, respectively, by assuming that the intersystem crossing (ISC) efficiency is close to unity for a simpler estimation.[40,58]

The non-radiative relaxation pathway of the excited state of **IrAu$_{12}$-b** is significantly suppressed compared to that of **IrAu$_{12}$-m** due to the rigid molecular structure of the bbpe ligand. The enlarged PL energy also contributes to the increase in k_r. The highly luminescent property of **IrAu$_{12}$-b** was achieved by both (1) accelerating the radiative process and (2) suppressing the non-radiative deactivation process. First, the acceleration of the radiative process is ascribed to the blue shift of the PL maximum, since the phosphorescence rate constant (k_p) is approximately proportional to the square of the radiation energy ($\bar{\nu}_0{}^2$) according to the relationship of $k_\mathrm{p} \approx \bar{\nu}_0{}^2 f_\mathrm{T}$, where f_T is the transition probability from T$_1$ to S$_0$. The f_T value depends on the transition probability from S$_0$ to S$_1$, the magnitude of spin–orbit coupling constant, and the S$_1$–T$_1$ splitting.[59,60] The absorption probabilities for **IrAu$_{12}$-b** and **IrAu$_{12}$-m** were comparable, due to the similar absorbance (Fig. S7†). The f_T value for **IrAu$_{12}$-b** should be increased due to the negligible S$_1$–T$_1$ splitting. The more symmetrical Ir@Au$_{12}$ core of **IrAu$_{12}$-b** likely enhances the orthogonality between the 1D to 1P superatomic orbitals, thereby strengthening the spin–orbit coupling.[61] The smaller S$_1$–T$_1$ splitting and the strengthened spin–orbit coupling thus contribute to the moderate increase in the k_r value.

Table 2 Photoluminescent properties and kinetic data of the deaerated solutions of IrAu$_{12}$-b and IrAu$_{12}$-m in CH$_2$Cl$_2$

	$\lambda_{\max}$ (nm)	τ (μs)	PLQY	k_r (s^{-1})	k_nr (s^{-1})
IrAu$_{12}$-b	596	4.18	0.870	2.1×10^5	3.1×10^4
IrAu$_{12}$-m (ref. 40)	736	3.6	0.135	3.7×10^4	2.4×10^5

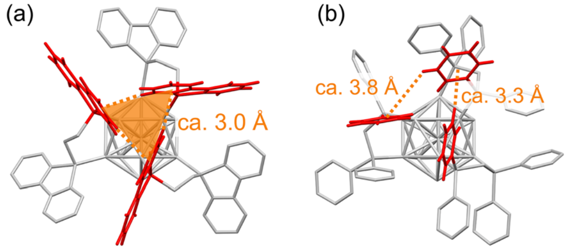

Fig. 4 Configuration of aromatic rings on the surface of (a) $IrAu_{12}$-b and (b) $IrAu_{12}$-m.

Second, the k_{nr} value of **$IrAu_{12}$-b** was drastically reduced, although the spin–orbit coupling also promotes the non-radiative deactivation.[60] Considering the independence of PLQY on the solvent polarity (Table S1†), the electrostatic interaction between the cationic Ir@Au_{12} core and the counter anion (PF_6^-) has little effect on the PLQY. Therefore, specific interactions between the ligands are expected. Fig. 4 shows the orientation of the aromatic rings in the ligand layers for **$IrAu_{12}$-b** and **$IrAu_{12}$-m**. The bbpe ligands are oriented so that each end faces the benzene ring of the adjacent one (Fig. 4a). The distances between the hydrogen atoms of a bbpe ligand and an aromatic ring of the adjacent one were estimated to be less than 3.1 Å, which is within the typical distance (2.7–3.2 Å) for the CH–π interaction of the edge-to-face aromatic conformation.[62] The restricted rotation of phenyl rings fixes the orientation of the bp units, which is advantageous for the bp ring to serve as both a CH donor and π acceptor. As a result, all the bp rings participate in the CH–π interaction network found in the outermost of **$IrAu_{12}$-b**. Three bp units form a triangular CH–π interaction network in a complementary manner, and eight stable triangles are formed at all the corners of the cuboidal cluster. The formation of the CH–π interaction network was also confirmed in the solution state by the ^1H NMR spectral change. Two broad peaks at 6.67 and 7.11 ppm could be assigned to the protons at the 3- and 4-positions of bp-units in **$IrAu_{12}$-b** (Fig. S4†). Those peaks were shifted upfield by more than 0.8 ppm relative to corresponding protons in the $Au_2(bbpe)Cl_2$ precursor due to the ring current effect by the bp unit of the adjacent ligand whereas other two peaks remain unchanged. Thus, the packing of bbpe ligands is solidified, which may also rigidify the central Ir@Au_{12} core, contributing to the suppression of non-radiative pathways and excited state structural relaxations, and the similar geometries of S_1 and T_1 states. On the other hand, such regular network interactions are absent in **$IrAu_{12}$-m**. While both CH–π and π–π interactions between densely packed phenyl groups are occasionally found, the avoidance of steric repulsions between phenyl rings with their rotational freedom seems to be prioritized.

Electrochemistry and electronic structures

The electrochemical measurement was carried out to experimentally determine the energy levels of HOMO and LUMO. Differential pulse voltammetry (DPV) clarified the first reduction (R1) and oxidation (O1) potentials (*vs.* Fc/Fc^+, Fc: ferrocene) for **$IrAu_{12}$-b** as −1.88 V and 0.76 V, and for **$IrAu_{12}$-m** as −1.94 V and 0.34 V, respectively (Fig. S8†). Although doping with a low-valent metal atom has been shown to decrease the O1 potential of MAu_{12} clusters,[35,40] the O1 potential of 0.76 V for **$IrAu_{12}$-b** is higher than those (0.4 and 0.74 V *vs.* Fc/Fc^+, respectively) of undoped $[Au_{13}(dppm)_6]^{5+}$ and $[Au_{13}(dppe)_5Cl_2]^{3+}$.[35,39] The electrochemical HL gaps (HL_e) for **$IrAu_{12}$-b** and **$IrAu_{12}$-m** were estimated to be 2.29 and 2.05 eV, by considering the charging energies (0.35 and 0.24 eV, respectively) estimated from the potential gaps between O1 and O2.[63] The HL_e values are consistent with the optical gap (HL_o) as shown in Fig. S8 and S9.† Thus, the large increase in the oxidation potential for **$IrAu_{12}$-b** results in the larger HL gap (2.29 eV). While the HL_o and PL energies are comparable with those of highly luminescent **$IrAu_{12}$-e-Cl**, the much larger O1 potential makes **$IrAu_{12}$-b** more tolerant toward the chemical oxidation of the Ir@Au_{12} core.[35]

The lowest singlet excited state (S_1) of most gold clusters undergoes rapid intersystem crossing to excited triplet states (T_n).[61] The energy differences between the S_1 and T_1 states (ΔE_{ST}) of **$IrAu_{12}$-m** and **$IrAu_{12}$-Cl-e** have been reported to be smaller than those of the undoped counterparts, probably because of the small structural difference between the S_1 and T_1 states[34,35] and the small exchange integral due to the presence of the heteroatom at the center of the superatom.[61] The ΔE_{ST} values estimated by DFT calculations for **$IrAu_{12}$-b** and **$IrAu_{12}$-m** were 0.007 and 0.08 eV, respectively (Fig. S10†). The smaller ΔE_{ST} value of **$IrAu_{12}$-b** should enhance the rate of the intersystem crossing,[35] further supporting our assumption of the quantitative ISC efficiency. The calculated T_1–S_0 gaps of **$IrAu_{12}$-b** and **$IrAu_{12}$-m** were 2.11 and 1.54 eV, respectively, which well reproduced the experimental PL energies (2.08 and 1.68 eV, respectively). The large PL blue-shift of **$IrAu_{12}$-b** is thus considered to originate from the expanded HL gap. The HOMO and LUMO of **$IrAu_{12}$-b** can be assigned to the superatomic 1P and 1D orbitals, respectively (Fig. 5 and S11†). The electronic structures of the gold clusters have been qualitatively explained by a jellium model in which the energy levels of the superatomic orbitals vary depending on the potential width and depth formed by the metal core.[64] Fig. S12† shows the DFT-optimized structures and the natural charges of **$IrAu_{12}$-b** and **$IrAu_{12}$-m**. The optimized structure of **$IrAu_{12}$-b** is highly symmetric (*T*-symmetry), while the symmetry of **$IrAu_{12}$-m** is reduced to S_6-symmetry by Jahn–Teller distortion. The natural charges for whole Ir@Au_{12} cores of **$IrAu_{12}$-b** and **$IrAu_{12}$-m** were estimated to be +0.53 and +0.57, respectively (Fig. S12†). The similar natural charges between the cores of **$IrAu_{12}$-b** and **$IrAu_{12}$-m** suggest the similar depth of the jellium potentials, which, in turn, cannot explain the difference in their HOMO levels.

The 1P and 1D superatomic orbitals of **$IrAu_{12}$-b** are more degenerated compared to those of **$IrAu_{12}$-m** (Fig. 5b). This trend can be explained by the higher symmetry of the Ir@Au_{12} core of **$IrAu_{12}$-b** (CSM = 0.032 for the optimized structure) and the higher symmetry of the phosphine coordination in **$IrAu_{12}$-b**, as described below. Five occupied orbitals below the 1P orbitals have the distinct contribution of the Ir 5d orbitals in a similar

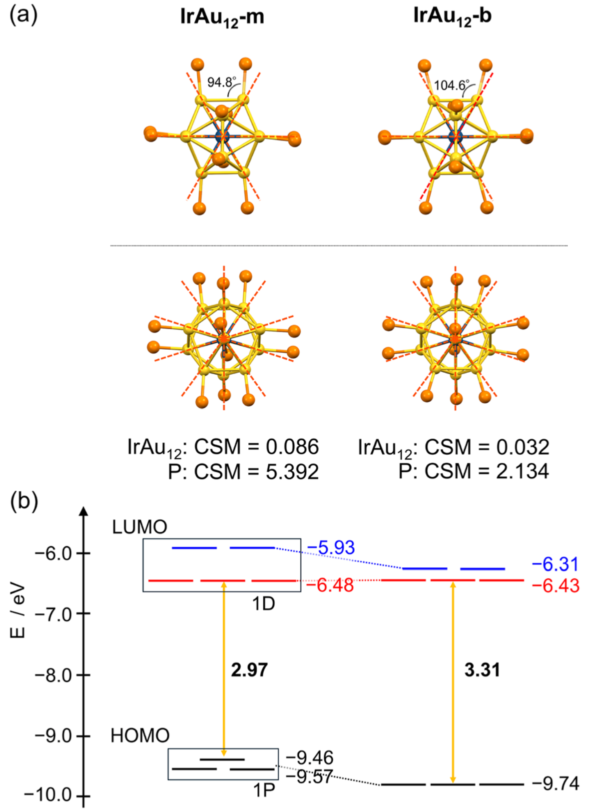

Fig. 5 (a) The positions of Au, Ir, and P atoms in the optimized structures of $IrAu_{12}$-m (left) and $IrAu_{12}$-b (right). The top and bottom panels show the view from an edge and a vertex direction of icosahedron, respectively. Color code: yellow, Au; dark blue, Ir; orange, P. (b) Energy levels of the Kohn–Sham orbitals of $IrAu_{12}$-m and $IrAu_{12}$-b estimated by DFT calculation.

manner to the electronic structure of **$IrAu_{12}$-Cl-e**.[33] Fig. 5a shows the positions of Ir, Au, and P atoms in the DFT-optimized structures of **$IrAu_{12}$-m** and **$IrAu_{12}$-b**. The superimposed orange dotted lines are the extension of the Ir–Au radial bonds and can be used as a measure to estimate the symmetry of the phosphine ligation. Clearly, the ligation symmetry in **$IrAu_{12}$-b** is higher than that in **$IrAu_{12}$-m**, since the P atoms of the former are located closer to the guide lines than those of the latter. Indeed, the Au–Au–P angle in **$IrAu_{12}$-b** was 104.6°, close to that expected for a perfect I_h coordination (120°), while that in **$IrAu_{12}$-m** was 94.8° (Fig. 5a). In addition, the CSM value for the P_{12} cage of **$IrAu_{12}$-b** (2.134) was smaller than that of **$IrAu_{12}$-m** (5.392), supporting that the phosphine ligands in **$IrAu_{12}$-b** coordinate more symmetrically to the Ir@Au_{12} core. As a result, the ligand field in **$IrAu_{12}$-b** is more spherical compared to **$IrAu_{12}$-m**, leading to the less energy splitting of the occupied 1P and unoccupied 1D superatomic orbitals (Fig. 5b).[48,65–67] Although further theoretical and experimental studies are needed to explain the change in the energy levels of the superatomic orbitals, we suggest that the higher I_h symmetry of the Ir@Au_{12} core and the more uniform surface ligation contribute to the larger HL gap for **$IrAu_{12}$-b**.

Conclusions

We used bis[benzo[*b*]phosphindole]ethane (bbpe) with a rigid molecular framework to stabilize the Ir@Au_{12} superatom. The use of bbpe ligands resulted in a hierarchically symmetric cluster: a nearly perfect Ir@Au_{12} core is capped by eight units of three bbpe ligands, circularly linked by CH–π interactions, arranged at the vertices of a cuboid. We observed interesting PL properties, including a relatively large PL energy (*ca.* 2.1 eV) and large PLQY (0.87), due to the symmetric structure with the rigidified core. These results demonstrate that a slight modification of the ligand structure results in a remarkable improvement of the PL properties of gold superatoms. The $[IrAu_{12}(bbpe)_6]^{3+}$ cluster with high T_1 energy together with the large oxidation potential, *i.e.* deep HOMO level, will find application as a photoredox catalyst.[35,37]

Data availability

The data supporting this article have been included as part of the ESI.†

Author contributions

K. Mutoh: conceptualization, data curation, validation, visualization, funding acquisition, writing–original draft, writing–review & editing. T. Yahagi & S. Kawakita: investigation, data curation. S. Takano: data curation, validation, methodology, writing–review & editing. T. Iwasa & T. Taketsugu: data curation, validation, writing–review & editing. T. Tsukuda: funding acquisition, data curation, methodology, resources, writing–review & editing. T. Nakashima: conceptualization, data curation, funding acquisition, resources, supervision, writing–review & editing. Each author contributed substantially to the manuscript.

Conflicts of interest

There are no conflicts to declare.

Acknowledgements

This work was financially supported by JST CREST (Grant Number: JPMJCR20B2), JSPS KAKENHI grant numbers JP22H05134 (TN) for Transformative Research (A) "Revolution of Chiral Materials Science using Helical Light", JP23H01938 (TN) and JP24K01458 (KM) for Scientific Research (B), and by Tokyo Ohka Foundation for The Promotion of Science and Technology and Kansai Research Foundation for Technology Promotion (KM). A part of this work was conducted in Institute for Molecular Science, supported by "Advanced Research Infrastructure for Materials and Nanotechnology in Japan (ARIM)" of the Ministry of Education, Culture, Sports, Science and Technology (MEXT). Proposal Number JPMXP1224MS0001. A part of calculations was performed using the Research Center for Computational Science, Okazaki, Japan.

Notes and references

1 M. Zhou, K. Li, Y. Pei, S. Jin and M. Zhu, *J. Phys. Chem. Lett.*, 2018, **14**, 11715–11724.
2 Q. Tang, G. Hu, V. Fung and D. Jiang, *Acc. Chem. Res.*, 2018, **51**, 2793–2802.
3 Y. Du, H. Sheng, D. Astruc and M. Zhu, *Chem. Rev.*, 2020, **120**, 526–622.
4 Y. Li and R. Jin, *J. Phys. Chem. C*, 2021, **125**, 15773–15784.
5 Y. Saito, C. Murata, M. Sugiuchi, Y. Shichibu and K. Konishi, *Coord. Chem. Rev.*, 2022, **470**, 214713.
6 X. Zou, X. Kang and M. Zhu, *Chem. Soc. Rev.*, 2023, **52**, 5892–5967.
7 J. Chen, P. Gu, G. Ran, Y. Zhang, M. Li, B. Chen, H. Lu, Y.-Z. Han, W. Zhang, Z. Tang, Q. Yan, R. Sun, X. Fu, G. Chen, Z. Shi, S. Wang, X. Liu, J. Li, L. Wang, Y. Zhu, J. Shen, B. Z. Tang and C. Fan, *Nat. Mater.*, 2024, **23**, 271–280.
8 R. Jin, H. Qian, Z. Wu, Y. Zhu, M. Zhu, A. Mohanty and N. Garg, *J. Phys. Chem. Lett.*, 2010, **1**, 2903–2910.
9 S. Bonacchi, S. Antonell, T. Dainese and F. Maran, *Chem.–Eur. J.*, 2021, **27**, 30–38.
10 Y. Shichibu, Y. Ogawa, M. Sugiuchi and K. Konishi, *Nanoscale Adv.*, 2021, **3**, 1005–1011.
11 W.-D. Si, C. Zhang, M. Zhou, W.-D. Tian, Z. Wang, Q. Hu, K.-P. Song, L. Feng, X.-Q. Huang, Z.-Y. Gao, C.-H. Tung and D. Sun, *Sci. Adv.*, 2023, **9**, eadg3587.
12 W.-D. Si, C. Zhang, M. Zhou, Z. Wang, L. Feng, C.-H. Tung and D. Sun, *Sci. Adv.*, 2024, **10**, eadm6928.
13 H. Yi, S. Song, S. M. Han, J. Lee, W. Kim, E. Sim and D. Lee, *Angew. Chem., Int. Ed.*, 2023, **62**, e202302591.
14 M. Mitsui, D. Arima, Y. Kobayashi, E. Lee and Y. Niihori, *Adv. Opt. Mater.*, 2022, **10**, 2200864.
15 S. Hossain, D. Hirayama, A. Ikeda, M. Ishimi, S. Funaki, A. Samanta, T. Kawawaki and Y. Negishi, *Aggregate*, 2023, **4**, e255.
16 P. Luo, X.-J. Zhai, S. Bai, Y.-B. Si, X.-Y. Dong, Y.-F. Han and S.-Q. Zang, *Angew. Chem., Int. Ed.*, 2023, **62**, e202219017.
17 M. Zhou, K. Li, Y. Pei, S. Jin and M. Zhu, *J. Phys. Chem. Lett.*, 2023, **14**, 11715–11724.
18 E. L. Albright, S. Malola, S. I. Jacob, H. Yi, S. Takano, K. Mimura, T. Tsukuda, H. Häkkinen, M. Nambo and C. M. Crudden, *Chem. Mater.*, 2024, **36**, 1279–1289.
19 T. I. Levchenko, H. Yi, M. D. Aloisio, N. K. Dang, G. Gao, S. Sharma, C.-T. Dinh and C. M. Crudden, *ACS Catal.*, 2024, **14**, 4155–4163.
20 K. Isozaki, K. Iseri, R. Saito, K. Ueda and M. Nakamura, *Angew. Chem., Int. Ed.*, 2024, **63**, e202312135.
21 Y. Shichibu and K. Konishi, *Small*, 2010, **6**, 1216–1220.
22 R. Jin, C. Liu, S. Zhao, A. Das, H. Xing, C. Gayathri, Y. Xing, N. L. Rosi, R. R. Gil and R. Jin, *ACS Nano*, 2015, **9**, 8530–8536.
23 Y. Yang, Q. Zhang, Z.-J. Guan, Z.-A. Nan, J.-Q. Wang, T. Jia and W.-W. Zhan, *Inorg. Chem.*, 2019, **58**, 3670–3675.
24 B. Jin, Y. Wang, C. Jin, J. J. De Yoreo and R. Tang, *J. Phys. Chem. Lett.*, 2021, **12**, 5938–5943.
25 J.-S. Yang, Y.-J. Zhao, X.-M. Li, X.-Y. Dong, Y.-B. Si, L.-Y. Xiao, J.-H. Hu, Z. Yu and S.-Q. Zang, *Angew. Chem., Int. Ed.*, 2024, **63**, e202318030.
26 P. H. Woodworth, M. F. Bertino, A. Ahmedb, A. Anwar, M. R. Shah, D. S. Wijesinghe and J. M. Pettibone, *Nano-Struct. Nano-Objects*, 2016, **7**, 32–40.
27 M. R. Narouz, S. Takano, P. A. Lummis, T. I. Levchenko, A. Nazemi, S. Kaappa, S. Malola, G. Yousefalizadeh, L. A. Calhoun, K. G. Stamplecoskie, H. Häkkinen, T. Tsukuda and C. M. Crudden, *J. Am. Chem. Soc.*, 2019, **141**, 14997–15002.
28 H. Yi, K. M. Osten, T. I. Levchenko, A. J. Veinot, Y. Aramaki, T. Ooi, M. Nambo and C. M. Crudden, *Chem. Sci.*, 2021, **12**, 10436–10440.
29 X. Yuan, Z. Ye, S. Malola, O. Shekhah, H. Jiang, X. Hu, J.-X. Wang, H. Wang, A. Shkurenko, J. Jia, V. Guillerm, O. F. Mohammed, X. Chen, N. Zheng, H. Häkkinen and M. Eddaoudi, *Chem. Sci.*, 2024, **15**, 16112–16117.
30 D. A. Buschmann, H. Hirai and T. Tsukuda, *Inorg. Chem. Front.*, 2024, **11**, 6694–6710.
31 H. Qian, D. Jiang, G. Li, C. Gayathri, A. Das, R. R. Gil and R. Jin, *J. Am. Chem. Soc.*, 2012, **134**, 16159–16162.
32 S. Chandra, A. Sciortino, S. Shandilya, L. Fang, X. Chen, N. H. Jiang, L.-S. Johansson, M. Cannas, J. Ruokolainen, R. H. A. Ras, F. Messina, B. Peng and O. Ikkala, *Adv. Opt. Mater.*, 2023, **11**, 2201901.
33 H. Hirai, S. Takano, T. Nakamura and T. Tsukuda, *Inorg. Chem.*, 2020, **59**, 17889–17895.
34 S. Takano and T. Tsukuda, *J. Am. Chem. Soc.*, 2021, **143**, 1683–1698.
35 H. Hirai, S. Takano, T. Nakashima, T. Iwasa, T. Taketsugu and T. Tsukuda, *Angew. Chem., Int. Ed.*, 2022, **61**, e202207290.
36 H. Hirai, T. Nakashima, S. Takano, Y. Shichibu, K. Konishi, T. Kawai and T. Tsukuda, *J. Mater. Chem. C*, 2023, **11**, 3095–3100.
37 H. Hirai, S. Takano, S. Masuda and T. Tsukuda, *ChemElectroChem*, 2024, **11**, e202300669.
38 W. Pei, L. Hou, J. Yang, S. Zhou and J. Zhao, *Nanoscale*, 2024, **16**, 14081–14088.
39 S.-S. Zhang, L. Feng, R. D. Senanayake, C. M. Aikens, X.-P. Wang, Q.-Q. Zhao, C.-H. Tung and D. Sun, *Chem. Sci.*, 2018, **9**, 1251–1258.
40 S. Takano, H. Hirai, T. Nakashima, T. Iwasa, T. Taketsugu and T. Tsukuda, *J. Am. Chem. Soc.*, 2021, **143**, 10560–10564.
41 M. Sugiuchi, Y. Shichibu, T. Nakanishi, Y. Hasegawa and K. Konishi, *Chem. Commun.*, 2015, **51**, 13519–13522.
42 Z.-H. Gao, J. Dong, Q.-F. Zhang and L.-S. Wang, *Nanoscale Adv.*, 2020, **2**, 4902–4907.
43 Y. Fukumoto, T. Omoda, H. Hirai, S. Takano, K. Harano and T. Tsukuda, *Angew. Chem., Int. Ed.*, 2024, **63**, e202402025.
44 Y. Shichibu, M. Zhang, T. Iwasa, Y. Ono, T. Taketsugu, S. Omagari, T. Nakanishi, Y. Hasegawa and K. Konishi, *J. Phys. Chem. C*, 2019, **123**, 6934–6939.
45 X. Wang, R. Liu, L. Tian, J. Bao, C. Zhao, F. Niu, D. Cheng, Z. Lu and K. Hu, *J. Phys. Chem. C*, 2022, **126**, 18374–18382.

46 L. Zeng, M. Zhou and R. Jin, *ChemPhysChem*, 2024, **25**, e202300687.

47 N. L. Smith and K. L. Knappenberger Jr, *J. Phys. Chem. A*, 2024, **128**, 7620–7627.

48 C. Yao, C.-Q. Xu, I.-H. Park, M. Zhao, Z. Zhu, J. Li, X. Hai, H. Fang, Y. Zhang, G. Macam, J. Teng, L. Li, Q.-H. Xu, F.-C. Chuang, J. Lu, C. Su, J. Li and J. Lu, *Angew. Chem., Int. Ed.*, 2020, **59**, 8270–8276.

49 P. Luo, X.-J. Zhai, S. Bai, Y.-B. Si, X.-Y. Dong, Y.-F. Han and S.-Q. Zang, *Angew. Chem., Int. Ed.*, 2023, **62**, e202219017.

50 E. L. Albright, T. I. Levchenko, V. K. Kulkarni, A. I. Sullivan, J. F. DeJesus, S. Malola, S. Takano, M. Nambo, K. Stamplecoskie, H. Häkkinen, T. Tsukuda and C. M. Crudden, *J. Am. Chem. Soc.*, 2024, **146**, 5759–5780.

51 X.-L. Pei, P. Zhao, H. Ube, Z. Lei, K. Nagata, M. Ehara and M. Shionoya, *J. Am. Chem. Soc.*, 2022, **144**, 2156–2163.

52 Z. Lei, M. Endo, H. Ube, T. Shiraogawa, P. Zhao, K. Nagata, X.-L. Pei, T. Eguchi, T. Kamachi, M. Ehara, T. Ozawa and M. Shionoya, *Nat. Commun.*, 2022, **13**, 4288.

53 X.-L. Pei, P. Zhao, H. Ube, Z. Lei, M. Ehara and M. Shionoya, *Nat. Commun.*, 2024, **15**, 5024.

54 B. M. Sutton, G. R. Girard, D. S. Eggleston, P. W. Baures, L. F. Faucette, R. K. Johnson and D. T. Hill, *J. Heterocycl. Chem.*, 1990, **27**, 1123–1126.

55 M. F. Bertino, Z.-M. Sun, R. Zhang and L.-S. Wang, *J. Phys. Chem. B*, 2006, **110**, 21416–21418.

56 Z. Wu, M. A. MacDonald, J. Chen, P. Zhang and R. Jin, *J. Am. Chem. Soc.*, 2011, **133**, 9670–9673.

57 K. Mutoh, S. Kawakita, T. Yahagi and T. Nakashima, *Nanoscale*, 2024, **16**, 21776–21782.

58 Z. Liu, M. Zhou, L. Luo, Y. Wang, E. Kahng and R. Jin, *J. Am. Chem. Soc.*, 2023, **145**(36), 19969–19981.

59 K. Schmidt, S. Brovelli, V. Coropceanu, D. Beljonne, J. Cornil, C. Bazzini, T. Caronna, R. Tubino, F. Meinardi, Z. Shuai and J.-L. Brédas, *J. Phys. Chem. A*, 2007, **111**(42), 10490–10499.

60 N. J. Turro , V. Ramamurthy and J. C. Scaiano, *Modern Molecular Photochemistry of Organic Molecules*, U Science, Sausalito, CA, 2010.

61 M. Mitsui, *J. Phys. Chem. Lett.*, 2024, **15**, 12257–12268.

62 H. Suezawa, T. Yoshida, Y. Umezawa, S. Tsuboyama and M. Nishio, *Eur. J. Inorg. Chem.*, 2002, 3148–3155.

63 D. Lee, R. L. Donkers, G. Wang, A. S. Harper and R. W. Murray, *J. Am. Chem. Soc.*, 2004, **126**, 6193–6199.

64 E. Janssens, S. Neukermans and P. Lievens, *Curr. Opin. Solid State Mater. Sci.*, 2004, **8**, 185–193.

65 S.-Y. Kang, Z.-A. Nan and Q.-M. Wang, *J. Phys. Chem. Lett.*, 2022, **13**, 291–295.

66 C. Liao, M. Zhu, D. Jiang and X. Li, *Chem. Sci.*, 2023, **14**, 4666–4671.

67 J.-X. Zhang, F. K. Sheong and Z. Lin, *Inorg. Chem.*, 2020, **59**, 8864–8870.